ADVANCED MATERIALS TECHNOLOGIES
www.advmattechnol.de

Efficient Gating of Organic Electrochemical Transistors with In-Plane Gate Electrodes

Dimitrios A. Koutsouras, Fabrizio Torricelli, Paschalis Gkoupidenis,* and Paul W. M. Blom**

Organic electrochemical transistors (OECTs) are electrolyte-gated transistors, employing an electrolyte between their gate and channel instead of an insulating layer. For efficient gating, non-polarizable electrodes, for example, Ag/AgCl, are typically used but unfortunately, this simple approach limits the options for multiple gate integration. Patterned polarizable Au gates on the other hand, show strongly reduced gating due to a large voltage drop at the gate/electrolyte interface. Here, an alternative, simple yet effective method for efficient OECT gating by scalable in-plane gate electrodes, is demonstrated. The fact that poly(3,4-ethylenedioxythiophene) polystyrene sulfonate (PEDOT:PSS) exhibits a volumetric capacitance in an electrolyte is made use of. As a result, the capacitance of PEDOT:PSS-based gates can be strongly enhanced by increasing their thickness, thereby reducing the voltage loss at the gate/electrolyte interface. By combining spin coating and electrodeposition, planar electrodes of various thicknesses are created on a multi-gated OECT chip and their effect on the gating efficiency, examined. It is shown that the gating performed by an in-plane PEDOT:PSS electrode can be tuned to be comparable to the one obtained by a Ag/AgCl electrode. Overall, the realization of efficient gating with in-plane electrodes paves the way toward integration of OECT-based biosensors and "organ-on-a-chip" platforms.

1. Introduction

Organic electrochemical transistors (OECTs) have recently gained tremendous popularity as building blocks for numerous applications in bioelectronics. OECTs belong to the class of electrolyte-gated organic transistors (EGOTs). They are three terminal devices with their semiconducting channel in contact with an ionically conducting and electronically insulating electrolyte (liquid or solid) which acts as the gate insulator.[1] Depending on their mode of operation, the EGOT channel can either be impermeable to the ions of the electrolyte or it can be permeable to them. OECTs make use of mixed ionic-electronic conducting polymers where ions can penetrate the channel and electrochemically dope or de-dope it. The prototypical conducting polymer poly(3,4-ethylenedioxythiophene) polystyrene sulfonate (PEDOT:PSS) is widely used as channel material. PEDOT:PSS is in contact with the gate electrode through the electrolyte and with source and drain electrodes measuring the channel's current.[2–4] Due to their operation mechanism, OECTs allow for the entire volume of the channel to participate in the current modulation resulting in a large transconductance.[5] The uniqueness of this architecture provides them with novel features. The absence of an insulating oxide layer, typically found in field-effect transistors, creates an ideal environment for direct integration of cell tissue on the device which acts as an amplifying transducer. An ionic event in the biological world changes the effective gate bias which in turn modulates the channel current. Hence, minute biological signals are enhanced and recorded through an OECT transconductance amplifier.[6] Their applications go beyond that, to sensing where OECTs have been used to sense barrier tissue integrity, especially for the most commonly used gastrointestinal model, the Caco-2 cell line.[7,8] They have also found applications in the active control of cell adhesion[9] and to cell-based biosensors[10] as well as the detection of analytes and metabolites.[11–13]

For the above applications, OECTs usually employ a non-polarizable Ag/AgCl electrode as gate. Such an electrode results in a Faradaic regime of operation for the device, where a large steady-state gate current changes the conducting state of the channel.[14,15] Nevertheless, a Ag/AgCl based gate limits the options for integrating more than one gate on the same chip, whereas OECT based neuromorphic circuits[16,17] or integrated sensing platforms[2,18–20] require multi-gate architectures with in-plane gates. An additional disadvantage when using the Ag/AgCl pellet electrode is that it needs to be suspended above

D. A. Koutsouras, P. Gkoupidenis, P. W. M. Blom
Department of Molecular Electronics
Max Planck Institute for Polymer Research
Ackermannweg 10, 55128 Mainz, Germany
E-mail: koutsouras@mpip-mainz.mpg.de; gkoupidenis@mpip-mainz.mpg.de; blom@mpip-mainz.mpg.de
F. Torricelli
Department of Information Engineering
University of Brescia
Via Branze 38, Brescia 25123, Italy

The ORCID identification number(s) for the author(s) of this article can be found under https://doi.org/10.1002/admt.202100732.

DOI: 10.1002/admt.202100732

the chip plane, rendering the device integration quite critical. Patterned polarizable gold (Au) or carbon (C) electrodes, on the other hand, show strongly reduced gating efficiency due to a large voltage drop at the gate/electrolyte interface.[14,15,21] In this case, the OECT operates in a non-Faradaic (capacitive) regime and, as a consequence, a small gate current is deployed to modulate the channel current. As a result, different gate modification processes needs to be applied for the modification of the C gate with electrodeposition of Au on it[21] or with the use of activated carbon (AC) as the gating material.[22]

Here, we demonstrate efficient OECT gating by patterned in-plane gate electrodes. Taking advantage of the fact that PEDOT:PSS exhibits a volumetric capacitance in an electrolyte, the capacitance of PEDOT:PSS-based gates can be strongly enhanced by increasing the polymer thickness, thereby reducing the voltage loss at the gate/electrolyte interface. By combining two different fabrication approaches, that is, spin coating and electrodeposition, we fabricated gate electrodes with various thicknesses on the same chip. By gating the same channel with electrodes of various capacitances, we reveal the effect of the gate film thickness on the gating efficiency. We show that the gating performance obtained with a PEDOT:PSS electrode can be tuned to be comparable to the one with a Ag/AgCl electrode. Using volumetric in-plane gates, we study the device physics of multi-gated OECTs revealing the role of the gate in the OECT operation. Our findings offer an additional degree of freedom in the designing of OECT-based biosensors and biosystems, opening opportunities for the simple yet effective integration of in-plane gate electrodes into multi-gate OECT architectures, and "organ-on-a-chip" platforms.

2. Results and Discussion

Figure 1a,b schematically presents the architecture of our devices. In both cases, there is a grid of 25 (5 lines × 5 rows) gate electrodes that were photolithographically patterned on selected positions and distances from the channel.

The area of each gate electrode is 2000 µm × 2000 µm and they are ordered along five lines with 7000 µm distance between them (*y*-axis). Along the *x*-axis, the gates are 3000 µm apart (Figure S1, Supporting Information). The difference between

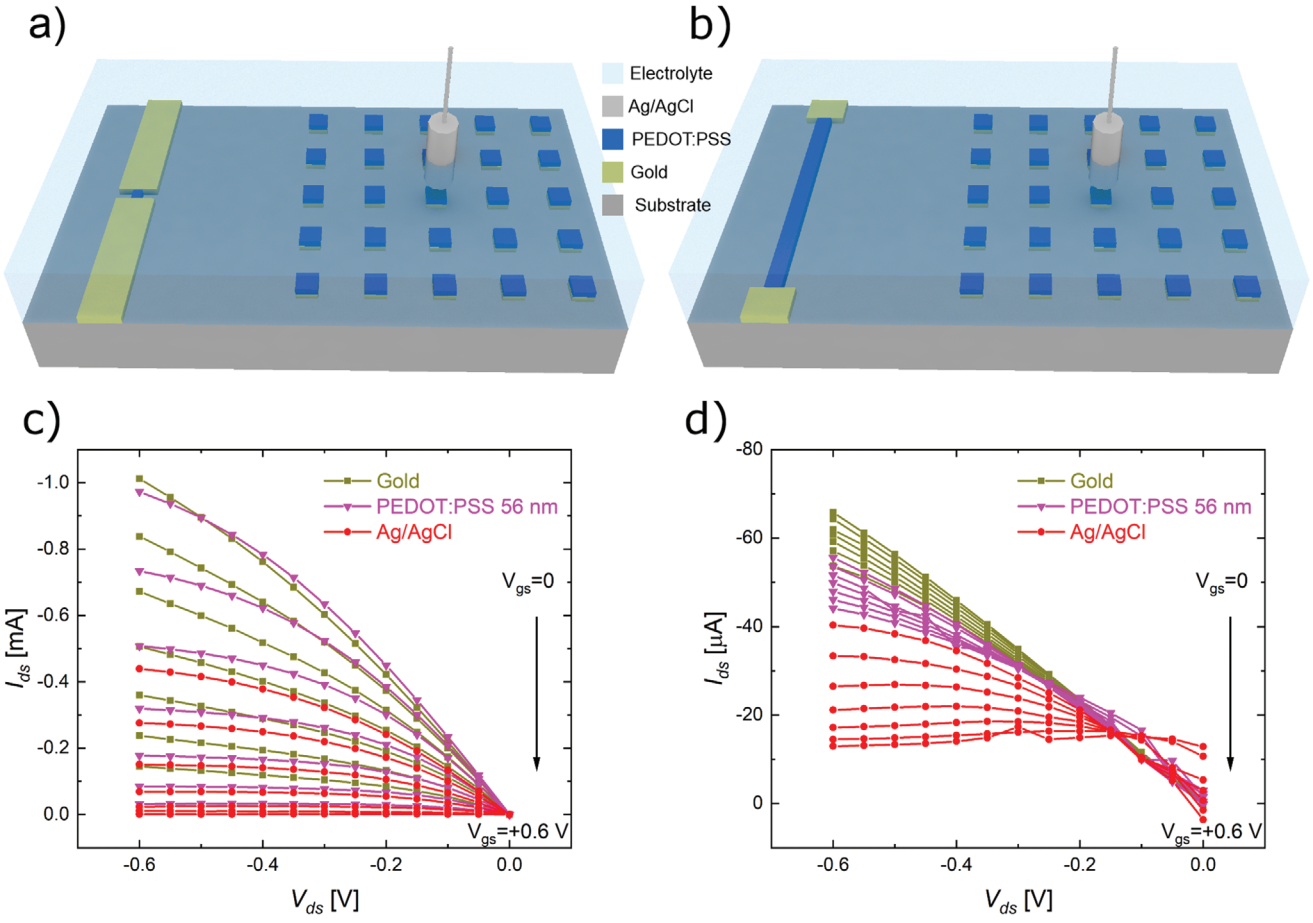

Figure 1. a,b) Schematic representation of the multi-gate OECT architectures (not in scale). The gate area is 2000 µm × 2000 µm. Small channel OECT. The channel dimensions are $W = 20$ µm and $L = 20$ µm. The ratio between the gate and channel area is $\lambda = 10^{-4}$ (a). Large channel OECT. The channel dimensions are $W = 500$ µm and $L = 15\,000$ µm and $\lambda \approx 1.9$ (b). c,d) The channel gating with in-plane gates consisting of a 56 nm thick PEDOT:PSS layer is more effective for the small λ (c) and less effective for the large channel (d). If the planar gate is replaced by a Ag/AgCl one, gating becomes effective in both cases. We note that a gold planar electrode can modulate the small channel current but this is not possible for the large one. The gate bias voltage sweeps from $V_{gs} = 0$ V to $V_{gs} = +0.6$ V with a voltage step equal to 0.05 V. Both figures show mean values of three measurements.

the two layouts is the size of the corresponding OECT channel. The small channel OECT (Figure 1a) has a width $W = 20$ µm and length $L = 20$ µm, which results in a channel area of 4×10^6 µm^2. Given that the gate electrode area is 4 10^6 µm^2, the ratio λ of the channel area to the gate area is small ($\lambda = \frac{A_{channel}}{A_{gate}} = 10^{-4}$) (Figure 1a). In the second structure (Figure 1b), a large channel with W = 500 µm and L = 15 000 µm provides λ = 1.875 and hence the OECT channel area is about two-times larger than the gate area (Figure 1b). In order to evaluate the effect of the gate electrode capacitance on gating, we first define the meaning of gating efficiency. The application of a positive gate bias depletes the channel from mobile positive charges near the drain driving the device into the saturation regime. The larger the applied gate bias is, the smaller the drain source voltage at which the channel is locally completely de-doped. A strongly increased gate capacitance reduces the voltage loss at the gate electrode such that the applied gate voltage drops exclusively at the electrolyte/channel interface. The result is that for a given positive gate bias, the channel current is more efficiently modulated with an increased gate capacitance. The ratio λ is an important device parameter as it determines the gating efficiency of the gate grid. Figure 1c,d shows that both the small and large channel, each with a thickness of 100 nm, can be gated by a 56 nm thick PEDOT:PSS gate electrode. However, we observe that the current can be modulated to a greater extent when λ is small. For large λ, the current modulation is small, even when a large positive potential (V_{gs} = +0.6 V) is applied at the gate.[23] Interestingly, the gating efficiency changes if a Ag/AgCl gate is used. In Figure 1c, Ag/AgCl modulates the source-drain current I_{ds} of the small channel, resulting in output curves analogous to the ones produced by the PEDOT:PSS gate electrode. Similarly, even in the case of the large channel, the use of the Ag/AgCl gate yields an improved current modulation (Figure 1d). In Figure 1c,d also, the output curves obtained with a gold gate electrode are presented. While for small λ, the channel current is modulated even with a 2000 µm × 2000 µm gold gate, for large λ, the modulation is negligible. Consequently, in the case of the large channel, the gating efficiency strongly depends on the choice of the material used for the gate electrode, as was also observed for various polarizable electrodes.[14]

To further deepen the analysis, we need to distinguish between two operation regimes. The Faradaic and non-Faradaic (or capacitive) one.[15] In the Faradaic regime, with the application of gate bias V_{gs}, reduction/oxidation (redox) reactions at the gate electrode result in a steady-state gate current in the electrolyte which drives ions in and out of the channel, thereby changing its conductivity. The non-Faradaic regime, on the other hand, is associated with the presence of a polarizable gate electrode. The application of a gate voltage V_{gs} now results in a transient current in the electrolyte through a charging mechanism of the gate double layer capacitor and a small gate current. As expected, gating is much more efficient for the Faradaic regime and this is the reason why the Ag/AgCl electrode is able to modulate the current for both channel sizes. Nevertheless, the OECT channel current measured for a small λ in Figure 1c implies that if the gate becomes big enough compared to the channel, gating from a polarizable electrode (Au) can become comparable to gating from a non-polarizable (Ag/AgCl) one. From a device physics point of view, it is not the area of the gate electrode that affects the gating efficiency, but rather its capacitance. The capacitance of the gate electrode C_g and the capacitance of the channel C_{Ch} can be considered as two capacitors in series, which can be combined into an equivalent capacitance C_{eq}.[3]

$$\frac{1}{C_{eq}} = \frac{1}{C_g} + \frac{1}{C_{Ch}} \quad (1)$$

It follows from Equation (1) that if we sufficiently increase the gate capacitance C_g, the term $\frac{1}{C_g}$ in Equation (1) can be neglected and therefore the gate electrode capacitor can be omitted from the device equivalent circuit. Then, the equivalent circuit simplifies into a simple series connection of R_s and C_{Ch}, where R_s accounts for the electrolyte spreading resistance, namely the solution ohmic resistance that depends on the electrolyte concentration and the size of the electrode. For a square electrode with length a, the spreading resistance is $R_s = \frac{\rho ln4}{\pi a}$, where ρ the solution resistivity.[24,25] In that case, it should be possible to achieve a channel current modulation similar to the one observed by a Ag/AgCl gate. Taking into account the fixed area of the patterned gate electrodes, a capacitance increase can be attained by increasing the PEDOT:PSS thickness (d) of the gate, as the former scales with the film volume (volumetric capacitance $C^* = 39$F/cm^3).[26] Increasing the thickness of the PEDOT:PSS gate electrode is expected to increase the gating efficiency. To this aim, the OECT fabrication process has to be adapted. On one side, spin coating is typically the method of choice for applying thin films of conducting polymers due to its simplicity and efficiency. Nevertheless, it comes with the restriction of an identical conducting polymer thickness all over the substrate, including the channel and the planar gates. On the other side, electrodeposition is a method that allows for the precise control of conducting polymer films thickness, but it requires an electrical conducting surface for the film formation. In this method, the PEDOT:PSS film is formed through an oxidative electrochemical driven reaction. Our approach is to combine the best of both methods, by using spin coating for the creation of the conducting polymer channel and electrodeposition to control the thicknesses of the gate electrodes. By that, we can engineer the channel geometry and control the thickness of each gate independently. As a result, this provides an extra degree of freedom in the device design. The thickness of the PEDOT:PSS channel (d) was chosen to be d = 100 nm while for the gate electrodes, four different thicknesses were selected, namely 56, 145, 233, and 454 nm. These electrodes, together with a bare gold one, were placed at the same distance (≈30 000 µm) from the channel (Figure S1, Supporting Information).

The capacitance of each gate electrode as a function of frequency was measured and the results are presented in **Figure 2**a. A gold electrode sized 2000 µm × 2000 µm is our point of reference. This electrode presents an almost constant capacitance value from 0.5 to 10^4 Hz. Nevertheless, the capacitance is rather small (less than a µF). We then increased the gate capacitance by electrodepositing a PEDOT:PSS film on the gold electrode. Addition of a 56 nm thick conducting polymer film results in a capacitance of ≈10 µF. By constantly increasing PEDOT:PSS film thickness, the capacitance also increases (Tables S1 and S2,

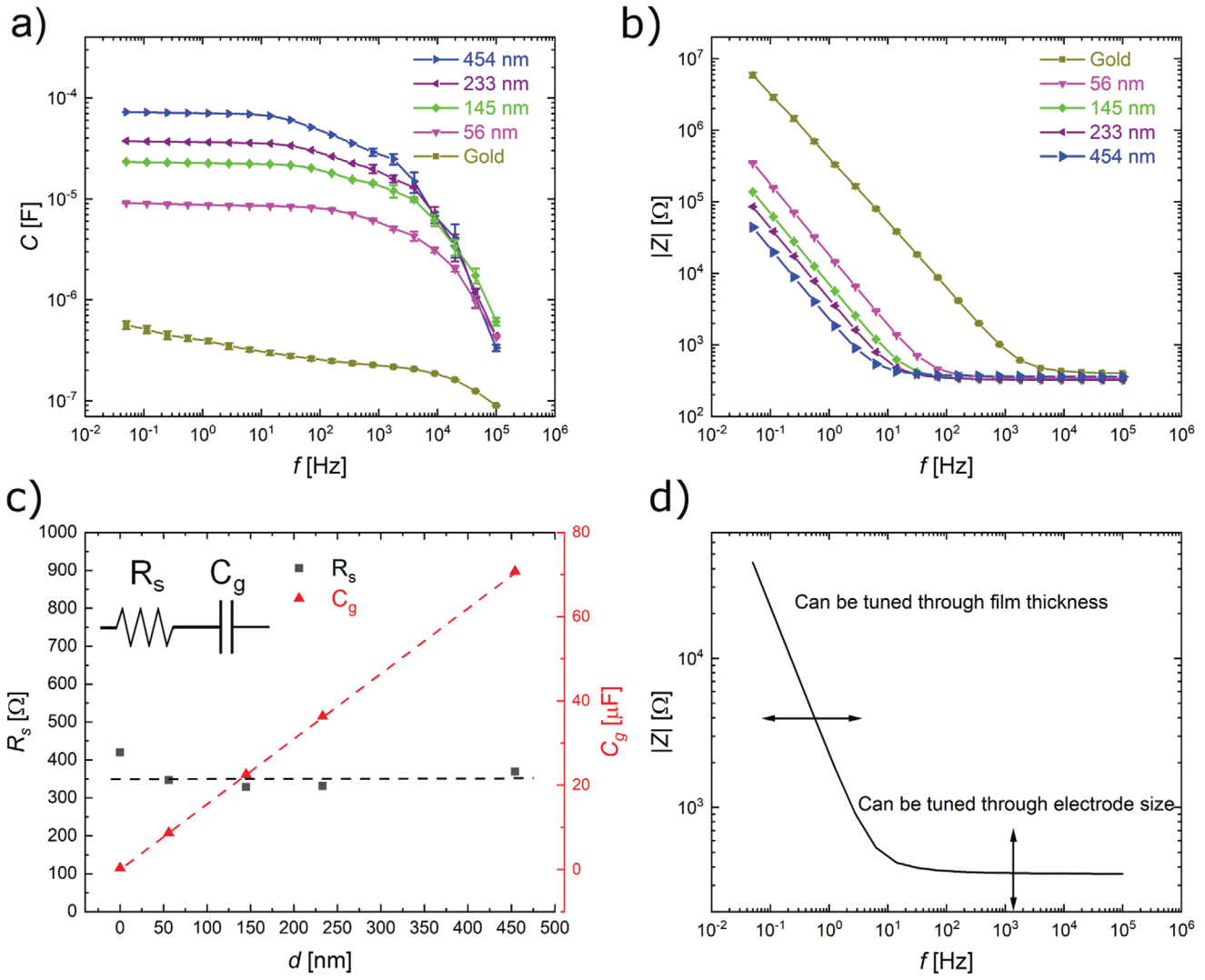

Figure 2. a) Capacitance as a function of frequency of bare gold electrode and gold electrodes covered with PEDOT:PSS of various thicknesses. b) Impedance spectra of the same electrodes. The resistive part at high frequencies is identical for every electrode because it depends only on the square root of its area. PEDOT:PSS thickness affects the electrode's capacitance as shown by the curve shift to lower frequencies. c) Variation of the spreading resistance R_s and capacitance C_g as a function of PEDOT:PSS film thickness d. R_s is constant for electrodes of the same size as it scales inversely with the square root of the area. Capacitance scales with thickness when the film area is constant. The lines serve as guide to the eye. d) The impedance spectrum of a PEDOT:PSS electrode can be shifted on demand on the impedance–frequency plane through an electrode size and thickness selection process. Figure 2a,b,c reports mean values ($n = 3$).

Supporting Information). The reason is the volumetric capacitance of PEDOT:PSS.[26] PEDOT:PSS is a conducting polymer that has been extensively used in bioelectronic applications. It consists of PEDOT-rich regions surrounded by PSS-rich regions.[27–29] The PEDOT:PSS film in contact with the electrolyte can be accessed by ions and a 3D polymer/electrolyte interface gives rise to an electrical double layer distributed in the whole volume of the polymer.

The gate capacitance scales with the PEDOT:PSS volume giving rise to a volumetric capacitance, as opposed to the double layer capacitance of polarizable metals in electrolytes.[30] Provided that the electrode area is fixed, the change of the PEDOT:PSS film thickness induces a linear change of the capacitance,[25] a fact which is used to calculate the film thickness in our study. A trade-off exists for the capacitance frequency dependence, as thicker films result in larger capacitance values at the cost of smaller cutoff frequency, meaning the frequency at which the electrodes capacitance starts to attenuate by −3dB. The impedance spectra of these PEDOT:PSS gate electrodes are presented in Figure 2b. At high frequencies, the spectra overlap independently of the conducting polymer thickness. This is in agreement with previously published work.[25,31] In the low-frequency regime, the increased electrode capacitance shifts the impedance cutoff frequency $f_c = \frac{1}{2\pi R_s C_g}$ to smaller values, namely the frequency at which a transition from a capacitive-dominated behavior (low frequencies) to a resistive-dominated behavior (high frequencies) in the device frequency response occurs. This means that thicker PEDOT:PSS films on the electrodes result in lower impedance

at the expense of a reduced cutoff frequency (slower system). In Figure 2c, the spreading resistance R_s and the capacitance C_g of the gate electrodes are plotted as a function of PEDOT:PSS thickness. The capacitance C_g scales with thickness, provided that the area is constant, while the spreading resistance R_s is independent of thickness, as it is a function of the square root of the electrode area.[25,26] The most striking result is the flexibility to tune the impedance spectrum of a PEDOT:PSS-based electrode by changing, on demand, its area and its thickness (Figure 2d). It has been already shown that at high frequencies, the impedance spectrum degenerates to an ohmic resistance spectrum (spreading resistance R_s) which scales inversely with the square root of the area of the electrode, corresponding to the length of the edge a in the case of a square electrode.[25] Thus, by altering the electrode's size, the resistive part of the spectrum shifts to larger or smaller impedance values. In this work, we show that by changing the PEDOT:PSS thickness, the cutoff frequency moves to higher or lower frequencies, which means that a capacitance change of the gate electrode shifts its impedance spectrum through the formula $f_c = \frac{1}{2\pi R_s C_g}$. (Figure 2d). Combining the two, the electrode impedance characteristics can be tuned to any position on the impedance-frequency plane, a fact that provides an extra degree of freedom in designing conducting polymer electrodes.

Most importantly, by changing the electrode's capacitance, we can tune its gating efficiency, as demonstrated in **Figure 3**. Figure 3a presents the output curves of a small channel device gated by PEDOT:PSS or Ag/AgCl electrodes. The Ag/AgCl electrode in NaCl electrolyte can be modeled as an ohmic resistance and it provides enhanced current modulation as compared to a polarizable Au electrode (Figure 1).[14,32]

As expected from Equation (1), the gate PEDOT:PSS thickness affects the output curves and the corresponding current modulation efficiency as displayed in Figure 3a. A gradual increase of the conducting polymer thickness results in a drain current curve that progressively resembles the one obtained when using a the Ag/AgCl electrode. The output curves measured with PEDOT:PSS of various thicknesses are presented in Figure S3, Supporting Information. The more efficient suppression of the channel current for positive gate bias is also visible in Figure 3b, which shows the corresponding transfer curves. A large gate capacitance due to increased PEDOT:PSS thickness results in a more efficient current modulation. For sufficiently thick films, the current modulation induced by an in-plane electrode approximates the one achieved by a Ag/AgCl gate. The above analysis is based on a small device where gating is quite efficient even for thin PEDOT:PSS films (e.g. 56 nm) and the reported values are mean values of three measurements. The error bars represent the standard deviation. Interestingly, for the large channel, the effect of an increasing gate capacitance on the gating efficiency is even more pronounced. Figure 3c shows the output curves obtained for two representative PEDOT:PSS gate thicknesses (56 and 454 nm) and a Ag/AgCl gate. The capacitance and impedance spectra of the various gate electrodes are reported in Figure S2, Supporting Information, while the corresponding output curves for all the PEDOT:PSS thicknesses are shown in Figure S4, Supporting Information. Again, the increasing PEDOT:PSS thickness results in output curves that gradually resemble the ones obtained by a Ag/AgCl electrode. Figure 3d shows the transfer curves for the large channel gated by a Ag/AgCl gate as well as multiple PEDOT:PSS gates of different thicknesses. As the PEDOT:PSS thickness on the gate electrode increases, its gating efficiency also increases, approaching the one of Ag/AgCl. The gate currents for a large channel as a function of the gate voltage is shown in Figure 3e. It is observed that the measured gate current increases with thickness, approaching (or exceeding) the Ag/AgCl gate current for thick films. In Figure 3f, the on/off ratio is plotted for the small and the large channel. The on/off ratio is indicative of an efficient current modulation, since it is defined as the ratio of the drain current at $V_g = 0$ V and $V_{ds} = -0.6$ V ("on-state" current) over the drain current at $V_g = +0.6$ V and $V_{ds} = -0.6$V ("off-state" current). For the small channel, the on/off ratio increases monotonically from 31, for PEDOT:PSS gate of 56 nm, to 190, for the 454 nm-thick gate, while the Ag/AgCl electrode provides the largest on/off ratio (357). For the large channel, the on/off ratio is significantly smaller due to the reduced current modulation and does not exceed 3.1, even for the Ag/AgCl gate electrode. Nevertheless, the trend that dictates an increase of the on/off ratio with gate thickness is always visible.

To investigate the impact of the PEDOT:PSS gate electrodes on the OECT performance, we measured the transconductance as a function of V_{gs} when a Ag/AgCl electrode and PEDOT:PSS electrodes are used (**Figure 4**). The transistor transconductance, defined as $g_m = \frac{\Delta I_{ds}}{\Delta V_{gs}}$, is a very relevant OECT figure of merit since it is directly related to the transistor signal amplification.[33] Interestingly, Figure 4 shows that the transconductance peak position depends on the gate thickness and this can be explained by Equation (1). The effective gate bias at the channel is governed by C_{eq} that can be tuned by means of C_g and C_{ch}. By changing from a non-polarizable to a polarizable gate electrode as well as by changing the gate capacitance with the PEDOT:PSS thickness of the polarizable gate electrode, we can simply and efficiently tune the OECT transconductance in terms of the peak position. The increase of the PEDOT:PSS gate thickness results in an increased gate capacitance that, in turn, reduces the voltage drop at the gate electrode. Consequently, ions from the solution are more efficiently injected inside the channel and de-dope it. As a result, the transfer curve becomes steeper as readily shown by the transconductance. We note that our approach is complementary to the transconductance engineering method based on the tuning of the OECT channel geometries, recently proposed by Rivnay and co-workers,[34] thus providing a new degree of freedom for the efficient and simple OECT performance optimization.

Figure 4a presents the case of a device with small ratio λ. The maximum transconductance for a 20 μm × 20 μm channel of 100 nm of thickness, gated by a Ag/AgCl electrode is obtained at $V_{gm,max} = -0.1$ V. In contrast, when a 56 nm thick PEDOT:PSS film is deposited on the planar Au gate, the maximum transconductance measured with the same OECT channel shifts to $V_{gm,max} = +0.1$ V. A further increase of the gate PEDOT:PSS thickness results in a shift of the g_m peak back to smaller gate voltage values. For a 454 nm film, the maximum transconductance value is achieved at $V_{gm,max} = 0$ V. The results are similar for a large λ device ($W = 500$ μm, $L = 1500$ μm, $d = 100$ nm).

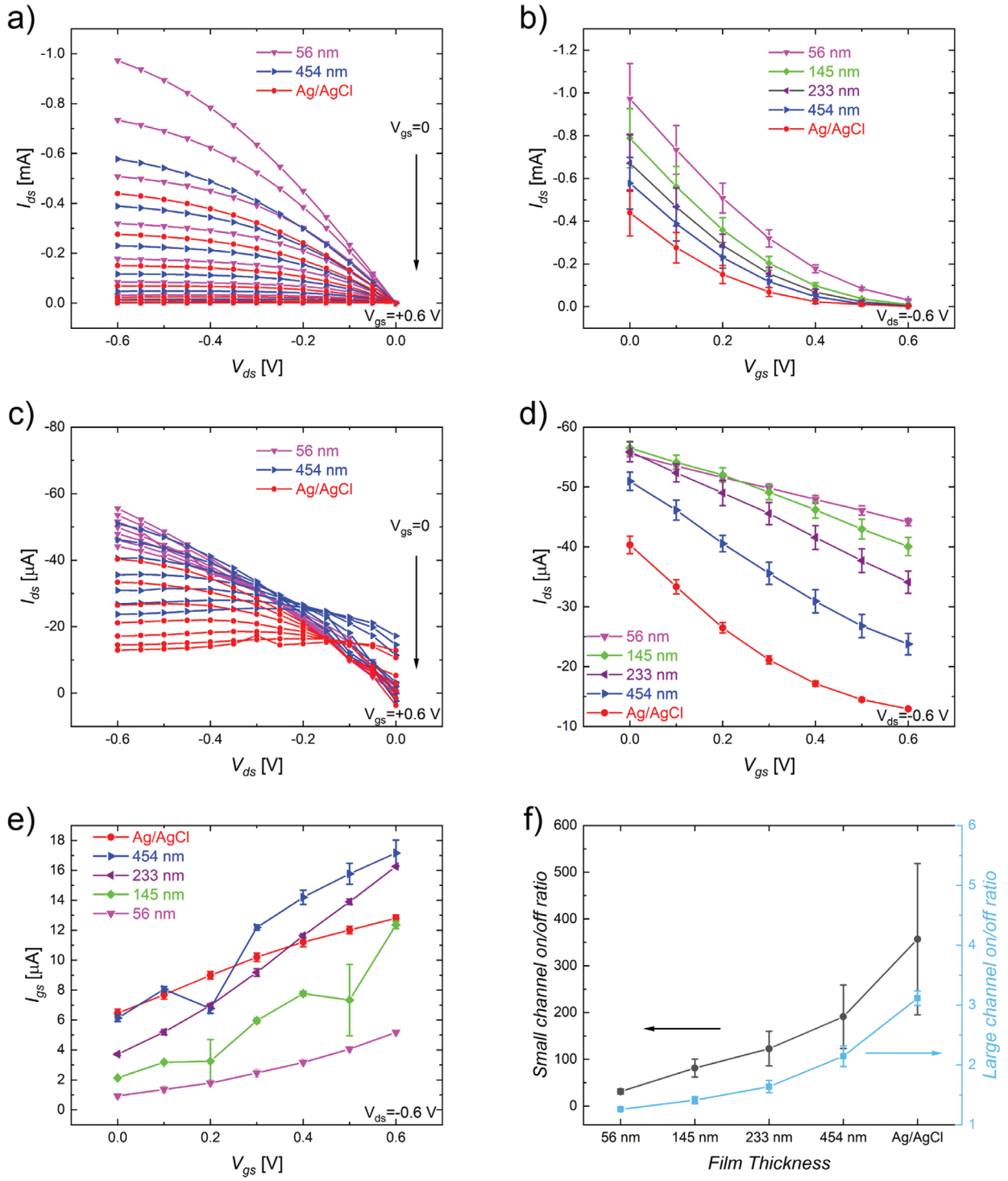

Figure 3. Effect of the electrode capacitance on its gating efficiency. a) Output curves of a small channel OECT gated by Ag/AgCl and PEDOT:PSS electrodes of two different thicknesses. Gate voltage sweeps from V_{gs} = 0 V to V_{gs} = +0.6 V. b) The transfer curves of the small channel transistor for drain bias V_{ds} = –0.6 V. c) Output curves of a large channel transistor gated by Ag/AgCl and PEDOT:PSS electrodes of two different thicknesses. Gate voltage sweeps from V_{gs} = 0 V to V_{gs} = +0.6 V. The increasing PEDOT:PSS thickness on the gate electrode leads, gradually, to a gating efficiency comparable to the one of Ag/AgCl. d) Transfer curves of a large channel OECT gated by PEDOT:PSS-based electrodes of different thicknesses for drain bias V_{ds} = –0.6 V. PEDOT:PSS thickness of the gate affects the gating efficiency. e) Steady-state gate current I_{gs} as a function of the gate voltage V_{gs} in the case of the large channel (V_{ds} = –0.6 V). I_{gs} increases with the increase of the gate thickness. f) The on/off ratios for the small and the large λ transistors. The overall trend is an increase of the on/off ratio with PEDOT:PSS film thickness. Ag/AgCl provides always the largest on/off values. The "on-state" current is measured at V_g = 0 V and V_{ds} = –0.6 V and the "off-state" current at V_g = +0.6 V and V_{ds} = –0.6 V. The plots show mean values (n = 3) and the error bars represent the standard deviation of the data.

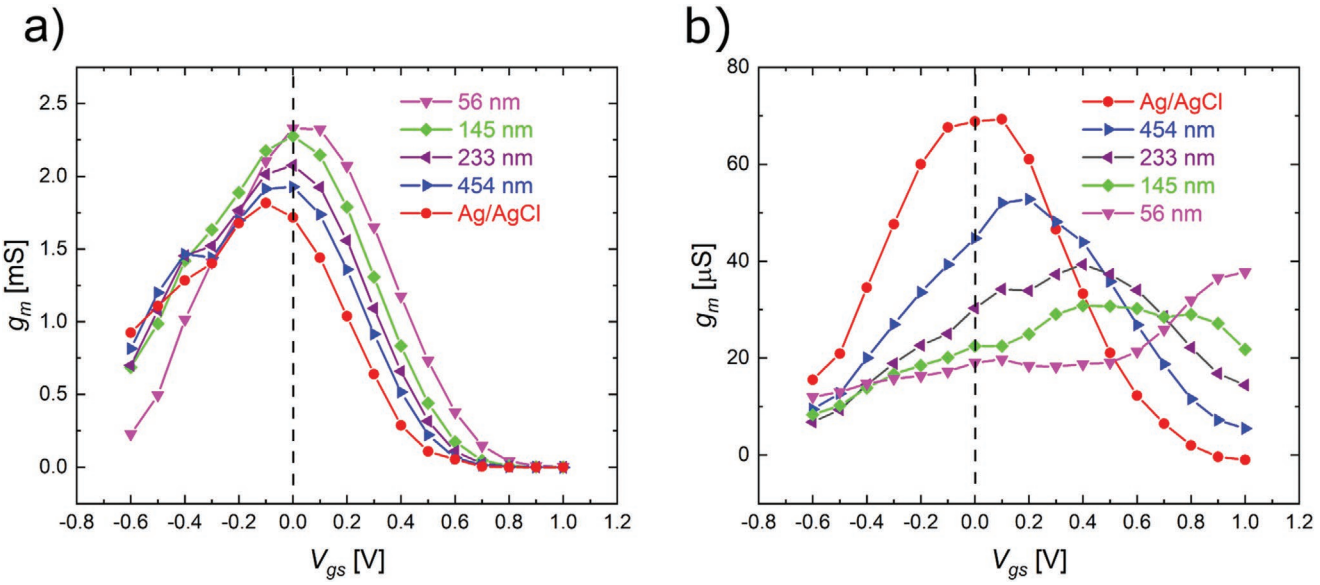

Figure 4. Transconductance engineering based on the gate PEDOT:PSS thickness. a) Small λ. The 20 µm × 20 µm device exhibits a maximum transconductance value at $V_{gm,max} = -0.1$ V when gated by a Ag/AgCl electrode. The replacement of Ag/AgCl with in-plane PEDOT:PSS electrodes shifts the $V_{gm,max}$ value to more positive values. As gate electrode thickness increases, the $V_{gm,max}$ moves back to less positive values and consequently it is possible to achieve maximum transconductance at $V_{gm,max} = 0$ V through a gate thickness selection process. b) The same trend appears for the large λ device ($W = 500$ µm, $L = 15\,000$ µm). By increasing the PEDOS:PSS thickness on the gate, the gate capacitance increases and the peak of the transconductance shifts closer to $V_{gs} = 0$ V. All the measurements are performed at $V_{ds} = -0.6$ V. The reported data are mean values ($n = 3$).

For thin PEDOT:PSS gates, the transconductance peaks at large and positive gate bias. Thicker PEDOT:PSS gates move the peak position to smaller gate biases Consequently, next to enhanced gating efficiency, the increase of the gate thickness also comes with the advantage of a decrease in the gate voltage at which the maximum transconductance is achieved. When the OECT channel volume is larger than the gate polymer volume, a significant voltage drop at the gate/electrolyte occurs and this results in a reduced g_m. Despite the fact that the volume of the channel is too large for the transconductance to peak at $V_{gm,max} = 0$ V, the overall trend is still visible. In both cases, small and large λ, the equivalent capacitance (Equation 1) determines the position of the transconductance peak. Therefore, the degree of freedom that comes with the control of the gate electrode film thickness allows for the simple yet effective tuning of the transconductance peak.

3. Conclusion

In conclusion, we present a micron-scale OECT that is efficiently gated with in-plane PEDOT:PSS gates of various thicknesses. The critical parameter for efficient gating is the ratio between the channel capacitance and the gate capacitance. Since the gate capacitance depends on the volume of the PEDOT:PSS layer on the gate, it can be strongly enhanced for thicker layers. By using a hybrid fabrication approach, which combines spin coating and electrodeposition, PEDOT:PSS film thickness is separately and accurately controlled on a grid of planar gate electrodes on the same chip. We show that thicker PEDOT:PSS gates demonstrate better gating capacity than their thinner counterparts. For sufficiently large gate capacitances, the gating efficiency of the planar PEDOT:PSS gate becomes comparable to the one of a Faradaic Ag/AgCl gate, which is typically used in OECTs biosensing applications. The comparative advantage of the in-plane electrode is that it can be easier integrated in biochips. Electrochemical impedance spectroscopy (EIS) measurements show that the characteristic of a PEDOT:PSS electrode can be shifted on demand on the impedance–frequency plane through an electrode size and thickness selection process. Furthermore, tuning the gate capacitance allows for fine tuning of the gate voltage at which the maximum transconductance is achieved. The ability to efficiently gate an OECT channel with in-plane gates adds an extra degree of freedom in the design of biosensors through a simplified operation scheme. Planar PEDOT:PSS gates can be easily integrated in bioelectronic OECT platforms, opening possibilities for multi-gate "organ-on-a-chip" solutions for biomedical applications.

4. Experimental Section

Materials: Poly(3,4-ethylenedioxythiophene) polystyrene sulfonate (PEDOT:PSS) (Clevios PH1000), Soap (Micro-90), 3,4-Ethylenedioxythiophene (EDOT), Poly(sodium4-styrene sulfonate) (PSSNa), Ethylene glycol, 4-dodecylbenzenesufonic acid (DBSA), and 3-methacryloxypropyltrimethoxysilane (GOPS) (Sigma–Alrich).

PEDOT:PSS formulation: 38 mL PEDOT:PSS, 2 mL of ethylene glycol (conductivity enhancement), 50 µL of 4-dodecylbenzenesufonic acid (DBSA) (film formation), and 0.4 mL of 3-methacryloxypropyltrimethoxysilane (GOPS) (surface adhesion promoter and polymer cross-linker agent).

Device Fabrication: The fabrication process combined two different approaches for the conducting polymer films patterning: spin-coating and electrodeposition. First, a fabrication protocol similar to the one reported before was used for the patterning of gold source, drain, and

gate electrodes.[35,36] Initially, 26 mm × 76 mm optical microscope glass slides were thoroughly cleaned in a soap (Micro-90) and subsequently in a 1:1 (v/v) solvent mixture (acetone/isopropanol) sonication bath. A first photolithography step (S1813 photoresist) patterned gold electrodes through a sputtering process (Pfeiffer-vacuum sputtering system). These electrodes were 100 nm thick and a 5 nm chromium layer promoted the adhesion of the electrodes on the substrate. The chips were then encapsulated with a double parylene C, 2 µm thick layer. Between the first layer and the substrate, Silane A-174 (gamma-methacryloxypropyltrimethoxysilane) was deposited to enhance the adhesion between them. On the contrary, soap solution (Micro-90, 1% v/v in distilled water) was spin-coated between the first and the second parylene C layer in order to facilitate the lift-off process in a subsequent fabrication phase. A second photolithography step followed (AZ 9260 photoresist). This step defined openings in the photoresist above the gate electrodes and the transistors' channels. Reactive ion etching (RIE) with O_2/CF_4 plasma was employed to remove parylene C under these windows to expose the gold electrodes and the device channel. PEDOT:PSS was spin-coated only between source and drain electrodes to create the conducting polymer channel. Finally, a peel-off step, defined the channel of the organic electrochemical transistor. After that, the devices were hard baked for an hour at 140 °C and placed in distilled water overnight for the removal of the excess of low molecular weight molecules from the channel. An electrodeposition protocol[25] was then used to create the PEDOT:PSS films of various thicknesses on the gate electrodes, from the 3,4-ethylenedioxythiophene (EDOT) monomer and poly(sodium4-styrene sulfonate) (PSSNa). Four different thicknesses were selected in order to study the effect of conducting polymer thickness on the gating efficiency. The Au electrodes were fabricated via gold sputtering (Pfeiffer-vacuum sputtering system). Ag/AgCl electrodes are cylinder pellets of 1.0 × 2.5 mm (D x L) (Warner Instruments).

Electropolymerization: The 3,4-ethylenedioxythiophen (EDOT) monomers were electrochemically polymerized to PEDOT:PSS from an aqueous solution that contained them together with poly(sodium4-styrene sulfonate) (PSSNa) in a ratio 1:10 (0.1 M PSSNa, 0.01 M EDOT). A steady current (galvanostatic mode) provided the reaction with required energy.[37]

Device Characterization and Measurements: Impedance spectroscopy measurements were performed with a potentiostat (PlamSens4) and a three-electrode configuration was adopted. The gate electrode served as the working electrode while a Ag/AgCl was the reference electrode and a Pt electrode was the counter electrode. The *I–V* characteristics of the transistors were obtained with a dual channel Keithley 2600 SMU.

Data Analysis: The recorded data were analyzed, modeled, and plotted with the help of Python, EIS Spectrum Analyser and Origin Ltd. The presented values are mean values of three measurements and the error bars represent the standard deviation of the data.

Supporting Information

Supporting Information is available from the Wiley Online Library or from the author.

Acknowledgements

Open access funding enabled and organized by Projekt DEAL.

Conflict of Interest

The authors declare no conflict of interest.

Data Availability Statement

The data that support the findings of this study are available from the corresponding author upon reasonable request.

Keywords

organic electrochemical transistors, device physics, organ-on-a-chip

Received: July 27, 2021
Published online:

[1] S. H. Kim, K. Hong, W. Xie, K. H. Lee, S. Zhang, T. P. Lodge, C. D. Frisbie, *Adv. Mater.* **2013**, *25*, 1822.
[2] D. A. Koutsouras, P. Leleux, M. Ramuz, J. Rivnay, G. G. Malliaras, in *2014 IEEE International Electron Devices Meet.*, IEEE, Piscataway, NJ **2014**, pp. 31.4.1–31.4.4.
[3] J. T. Friedlein, R. R. McLeod, J. Rivnay, *Org. Electron.* **2018**, *63*, 398.
[4] J. Rivnay, S. Inal, A. Salleo, R. M. Owens, M. Berggren, G. G. Malliaras, *Nat. Rev. Mater.* **2018**, *3*, 17086.
[5] D. Khodagholy, J. Rivnay, M. Sessolo, M. Gurfinkel, P. Leleux, L. H. Jimison, E. Stavrinidou, T. Herve, S. Sanaur, R. M. Owens, G. G. Malliaras, *Nat. Commun.* **2013**, *4*, 2133.
[6] D. Khodagholy, T. Doublet, P. Quilichini, M. Gurfinkel, P. Leleux, A. Ghestem, E. Ismailova, T. Hervé, S. Sanaur, C. Bernard, G. G. Malliaras, *Nat. Commun.* **2013**, *4*, 1575.
[7] L. H. Jimison, S. A. Tria, D. Khodagholy, M. Gurfinkel, E. Lanzarini, A. Hama, G. G. Malliaras, R. M. Owens, *Adv. Mater.* **2012**, *24*, 5919.
[8] L. V. Lingstedt, M. Ghittorelli, M. Brückner, J. Reinholz, N. I. Crăciun, F. Torricelli, V. Mailänder, P. Gkoupidenis, P. W. M. Blom, *Adv. Healthcare Mater.* **2019**, *8*, 1900128.
[9] M. H. Bolin, K. Svennersten, D. Nilsson, A. Sawatdee, E. W. H. Jager, A. Richter-Dahlfors, M. Berggren, *Adv. Mater.* **2009**, *21*, 4379.
[10] P. Lin, F. Yan, J. Yu, H. L. W. Chan, M. Yang, *Adv. Mater.* **2010**, *22*, 3655.
[11] N. Wang, A. Yang, Y. Fu, Y. Li, F. Yan, *Acc. Chem. Res.* **2019**, *52*, 277.
[12] P. Lin, F. Yan, *Adv. Mater.* **2012**, *24*, 34.
[13] Z.-T. Zhu, J. T. Mabeck, C. Zhu, N. C. Cady, C. A. Batt, G. G. Malliaras, *Chem. Commun.* **2004**, 1556.
[14] G. Tarabella, C. Santato, S. Y. Yang, S. Iannotta, G. G. Malliaras, F. Cicoira, *Appl. Phys. Lett.* **2010**, *97*, 123304.
[15] F. Lin, M. C. Lonergan, *Appl. Phys. Lett.* **2006**, *88*, 133507.
[16] P. Gkoupidenis, D. A. Koutsouras, T. Lonjaret, J. A. Fairfield, G. G. Malliaras, *Sci. Rep.* **2016**, *6*, 27007.
[17] P. Gkoupidenis, S. Rezaei-Mazinani, C. M. Proctor, E. Ismailova, G. G. Malliaras, *AIP Adv.* **2016**, *6*, 111307.
[18] S. Wustoni, C. Combe, D. Ohayon, M. H. Akhtar, I. McCulloch, S. Inal, *Adv. Funct. Mater.* **2019**, *29*, 1904403.
[19] F. Decataldo, M. Barbalinardo, M. Tessarolo, V. Vurro, M. Calienni, D. Gentili, F. Valle, M. Cavallini, B. Fraboni, *Adv. Mater. Technol.* **2019**, *4*, 1900207.
[20] V. F. Curto, B. Marchiori, A. Hama, A.-M. Pappa, M. P. Ferro, M. Braendlein, J. Rivnay, M. Fiocchi, G. G. Malliaras, M. Ramuz, R. M. Owens, *Microsyst. Nanoeng.* **2017**, *3*, 17028.
[21] M. Sensi, M. Berto, A. Candini, A. Liscio, A. Cossarizza, V. Beni, F. Biscarini, C. A. Bortolotti, *ACS Omega* **2019**, *4*, 5374.
[22] H. Tang, P. Kumar, S. Zhang, Z. Yi, G. D. Crescenzo, C. Santato, F. Soavi, F. Cicoira, *ACS Appl. Mater. Interfaces* **2015**, *7*, 969.
[23] F. Cicoira, M. Sessolo, O. Yaghmazadeh, J. A. DeFranco, S. Y. Yang, G. G. Malliaras, *Adv. Mater.* **2010**, *22*, 1012.
[24] D. A. Bernards, G. G. Malliaras, *Adv. Funct. Mater.* **2007**, *17*, 3538.
[25] D. A. Koutsouras, P. Gkoupidenis, C. Stolz, V. Subramanian, G. G. Malliaras, D. C. Martin, *ChemElectroChem* **2017**, *4*, 2321.
[26] J. Rivnay, P. Leleux, M. Ferro, M. Sessolo, A. Williamson, D. A. Koutsouras, D. Khodagholy, M. Ramuz, X. Strakosas, R. M. Owens, C. Benar, J.-M. Badier, C. Bernard, G. G. Malliaras, *Sci. Adv.* **2015**, *1*, e1400251.

[27] A. M. Nardes, M. Kemerink, R. A. J. Janssen, J. A. M. Bastiaansen, N. M. M. Kiggen, B. M. W. Langeveld, A. J. J. M. van Breemen, M. M. de Kok, *Adv. Mater.* **2007**, *19*, 1196.
[28] U. Lang, E. Müller, N. Naujoks, J. Dual, *Adv. Funct. Mater.* **2009**, *19*, 1215.
[29] C. M. Palumbiny, C. Heller, C. J. Schaffer, V. Körstgens, G. Santoro, S. V. Roth, P. Müller-Buschbaum, *J. Phys. Chem. C* **2014**, *118*, 13598.
[30] C. M. Proctor, J. Rivnay, G. G. Malliaras, *J. Polym. Sci., Part B: Polym. Phys.* **2016**, *54*, 1433.
[31] J. Newman, *J. Electrochem. Soc.* **1966**, *113*, 501.
[32] A. J. Bard, L. R. Faulkner, *Electrochemical methods: Fundamentals and applications*, Wiley, New York **1980**.
[33] F. Torricelli, L. Colalongo, D. Raiteri, Z. M. Kovács-Vajna, E. Cantatore, *Nat. Commun.* **2016**, *7*, 10550.
[34] J. Rivnay, P. Leleux, M. Sessolo, D. Khodagholy, T. Hervé, M. Fiocchi, G. G. Malliaras, *Adv. Mater.* **2013**, *25*, 7010.
[35] M. Sessolo, D. Khodagholy, J. Rivnay, F. Maddalena, M. Gleyzes, E. Steidl, B. Buisson, G. G. Malliaras, *Adv. Mater.* **2013**, *25*, 2135.
[36] D. A. Koutsouras, A. Hama, J. Pas, P. Gkoupidenis, B. Hivert, C. Faivre-Sarrailh, E. Di Pasquale, R. M. Owens, G. G. Malliaras, *MRS Commun.* **2017**, *7*, 259.
[37] X. Cui, D. C. Martin, *Sens. Actuators, B* **2003**, *89*, 92.